J Nanopart Res (2017) 19: 35
DOI 10.1007/s11051-016-3736-z

RESEARCH PAPER

Controllable synthesis of p-type Cu_2S nanowires for self-driven NIR photodetector application

Chun-Yan Wu · Zhi-Qiang Pan · Zhu Liu · You-Yi Wang · Feng-Xia Liang · Yong-Qiang Yu · Li Wang · Lin-Bao Luo

Received: 21 March 2016 / Accepted: 30 December 2016 / Published online: 18 January 2017

Abstract Face-centered cubic Cu_2S nanowires with length of up to 50 μm and diameters in the range of 100–500 nm are synthesized on Si substrates through the chemical vapor deposition method using a mixed gas of Ar and H_2 as the carrier gas under a chamber pressure of about 700 Torr. It was found that the growth of quasi 1D nanostructure followed a typical vapor-liquid-solid (VLS) mechanism in which the element Cu was reduced by H_2 as the catalyst. The as-synthesized Cu_2S nanowires exhibited typical p-type semiconducting characteristics with a conductivity of about 600 S cm^{-1} and a hole mobility (μ_h) of about 72 cm^2 V^{-1} s^{-1}. Further study reveals that p-Cu_2S nanowires/n-Si heterojunction exhibits distinct rectifying characteristics with a turn-on voltage of ~0.6 V and a rectification ratio of ~300 at ±1 V in the dark and a pronounced photovoltaic behavior with an open circuit voltage (V_{oc}) of 0.09 V and a short circuit current (I_{sc}) of 65 nA when illuminated by the NIR light (790 nm, 0.35 mW cm^{-1}), giving rise to a responsivity (R) about 0.8 mA W^{-1} and specific detectivity (D^*) 6.7×10^{10} cm $Hz^{1/2}$ W^{-1} at zero bias, which suggests the potential of as-synthesized Cu_2S nanowires applied in the field of self-driven NIR photodetector.

Keywords Semiconductor nanostructures · Heterojunction · Self-driven NIR photodetector · Responsivity · Specific detectivity · Nanoelectronics

C.-Y. Wu (✉) · Z.-Q. Pan · Z. Liu · Y.-Y. Wang · Y.-Q. Yu · L. Wang · L.-B. Luo (✉)
School of Electronic Science and Applied Physics, Hefei University of Technology, Hefei, Anhui 230009, People's Republic of China
e-mail: cywu@hfut.edu.cn
e-mail: luolb@hfut.edu.cn

F.-X. Liang
School of Materials Science and Engineering and Anhui Provincial Key Laboratory of Advanced Functional Materials and Devices, Hefei University of Technology, Hefei, Anhui 230009, People's Republic of China

Introduction

Copper sulfide (Cu_xS) is an earth-abundant and environmentally benign transition metal chalcogenide which can exist in five stable phases at room temperature according to the phase diagram of the Cu-S system: covellite CuS, djurleite $Cu_{1.95}S$, digenite $Cu_{1.8}S$, anilite $Cu_{1.75}S$, and chalcocite Cu_2S (Adelifard et al. 2012). They have been widely used in fields such as photovoltaic devices (Garnett et al. 2009), photoelectric devices (Su et al. 2013), photocatalysis (An et al. 2015), photothermal therapy agents (Tian et al. 2011), gas sensors (Bo et al. 2010), and cathode materials in lithium batteries (Lai et al. 2010a, b). Meanwhile, unique properties may also arise from their rich structures and components. For example, Cu_2S is known to be a good candidate for solar cell applications due to its p-type conductivity with shallow Cu vacancy acceptors and ideal bulk band gap (1.2 eV at room temperature) (Fahrenbruch and Bube 1983). $Cu_{2-x}S$, a fast superionic conductor with structural disorder, is a potential material in the field of thermoelectric and photoelectric transformers and high-temperature thermistors (Zhao et al. 2009). CuS displays metallic

conductivity and transforms at 1.6 K into a superconductor (Zhang et al. 2003).

To date, a number of methods, including solution-based approaches such as solvothermal (Liu et al. 2005) and electrochemical methods (Ghahremaninezhad et al. 2011), have been used in the synthesis of copper sulfide nanostructures, such as nanoparticles (Xiong et al. 1998), microspheres (Thongtem et al. 2010), nanoflakes (Mu et al. 2010), nanodisks (Lim et al. 2006), nanowires (Wu et al. 2008), and dendrites (Wu et al. 2006a, b). However, due to the enrichment of chemical compositions and phases, facial synthesis of single-phase copper sulfide with controllable transport property still remains to be a challenge (Wang et al. 2007). Crystalline Cu_2S nanowire arrays were firstly grown on copper surface through a solid-gas reaction in O_2/H_2S under ambient conditions (Wang and Yang 2001). To avoid the usage of the toxic gas H_2S, Chen et al. used sulfur as the starting materials and ethylenediamine (EDA) and hydrazine in alkali solution as the reduction scheme (Lai et al. 2010a, b). However, the unintentional interfacial defect commonly present on the surface of nanostructures fabricated by a low-temperature solution-based approach (Wang et al. 2009) will definitely degrade their electrical performance such as conductivity and thus will hinder their application in the field of nanodevices.

Chemical vapor deposition (CVD) has achieved great success in the synthesis of semiconductor nanostructures including many transitional metal sulfides (Zhai et al. 2011; Bierman et al. 2008), but only few research on the synthesis of Cu_xS nanostructures have been reported, which may also be attributed to their abundant chemical compositions and phases. Yuan et al. have reported the controllable growth of CuS nanowalls with a thin layer of $Cu_{2-x}S$ nanoparticles on the bottom (Feng et al. 2007). Zero-dimensional (0D) octahedral $Cu_{1.96}S$ single crystal, one-dimensional (1D) $Cu_{1.96}S$ nanorod, and two-dimensional (2D) hexagonal CuS nanoflakes have been controllable synthesized in a home-built horizontal CVD reactor through the temperature-dependent crystal growth mechanism (Xu et al. 2012). To the best of our knowledge, a facial approach to the synthesis of Cu_2S single crystal nanostructures still needs to be researched. Herein, we report the controllable synthesis of pure single crystal Cu_2S nanowires through a CVD method, using CuCl and S as the copper source and sulfur source, respectively. Electrical characterization reveals the as-synthesized nanowires to be p-type semiconductor with a hole mobility 72 $cm^2\ V^{-1}\ s^{-1}$. Further device analysis shows that the p-Cu_2S/n-Si heterojunction exhibits remarkable photovoltaic properties and can function as a high-performance self-driven NIR photodetector with good reproducibility.

Experiment

Synthesis and structural characterization of Cu_2S nanowires

All the reagents (analytical-grade purity) were purchased from Shanghai Chemical Reagents Co. and were used without any further purification. The synthesis of the Cu_2S nanowires was conducted in a horizontal tube furnace via a simple thermal co-evaporation method. In a typical synthesis of Cu_2S nanowires, 0.3 g S powder and 0.1 g CuCl powder were loaded into two separated alumina boats and transferred to the upstream region and center region (the heating zone) of the furnace, respectively. The distance between the two boats was about 9 cm. n-type Si wafers (30 mm × 10 mm) with a resistivity of 4–7 $\Omega\ cm^{-1}$ were then placed at the downstream position about 5 cm away from CuCl source, as illustrated in Fig. 1. The reaction chamber was flushed and filled with a mixture gas of Ar and H_2 (with the flow rate of 10 and 50 sccm, respectively, sccm denotes standard cubic centimeter per minute) after evacuated to a base pressure of 6×10^{-3} Pa. The pressure in the chamber was adjusted to 700 Torr before heating. Thereafter, the furnace was heated up to 700 °C with a heating rate of 20 °C min^{-1} and maintained

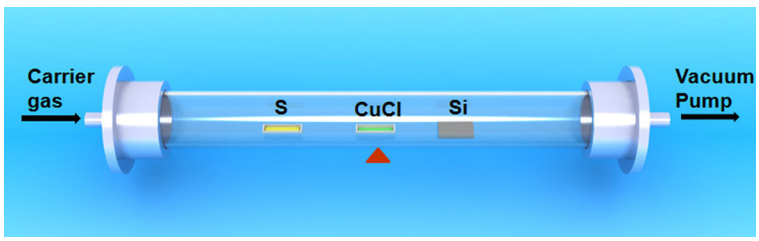

Fig. 1 Schematic illustration for the synthesis of Cu_2S nanowires

at that temperature for about 50 min. After the system was cooled down to room temperature, the Si substrates with a layer of black product were taken out of the furnace.

The morphologies and structures of the as-synthesized Cu_2S nanowires were characterized by X-ray diffraction (XRD, Rigaku D/MAX-γB, Cu Kα radiation, λ = 1.54178 Å), field emission scanning electron microscopy (FESEM, SIRION 200FEG), and high-resolution transmission electron microscopy (HRTEM, JEOL-2010, at 200 kV). The chemical composition of the products was detected by the energy-dispersive X-ray spectroscopy (EDS, Oxford INCA, attached to SEM). The UV–vis spectrum was performed on a UV–vis spectrometer (CARY 5000). The Raman analysis was performed on a Raman spectrometer (HORIBA JOBIN YVON, LabRam HR Evolution) using an excitation wavelength 532 nm from an Ar ion laser. X-ray photoelectron (XPS) spectra were recorded on a Thermo ESCALAB250 X-ray photoelectron spectrometer using monochromatized Al Kα X-ray as the excitation source.

Device fabrication and analysis

To assess the electrical properties of the Cu_2S nanowires, bottom-gate field-effect transistors (FETs) based on an individual Cu_2S nanowire were constructed. Briefly, the as-synthesized Cu_2S nanowires were dispersed on a SiO_2 (300 nm)/n^+-Si substrate. Then photolithography, electron beam deposition, and a subsequent lift-off process were utilized to define the Au (50 nm) electrodes on the Cu_2S nanowires. During device analysis, the heavily doped Si substrate acted as the global bottom gate in the nanoFETs. For the electrical characterization of the p-Cu_2S/n-Si heterojunction, the Au (50 nm) electrodes were deposited onto the as-grown Cu_2S layer on the n-Si substrate with a shadow mask. All the electrical measurements were carried out at room temperature with a semiconductor characterization system (Keithley 4200-SCS).

Results and discussion

Figure 2a shows a typical XRD pattern of the as-synthesized products. All the diffraction peaks can be well indexed to face-centered cubic Cu_2S phase (JCPDS card no. 84-1770). No evident impurity peaks from Cu and Cu_2O are observed, indicating that the products are of single phase and high purity. The typical SEM image of the as-synthesized Cu_2S nanowires is presented in Fig. 2b, showing a general morphology of nanowires with length

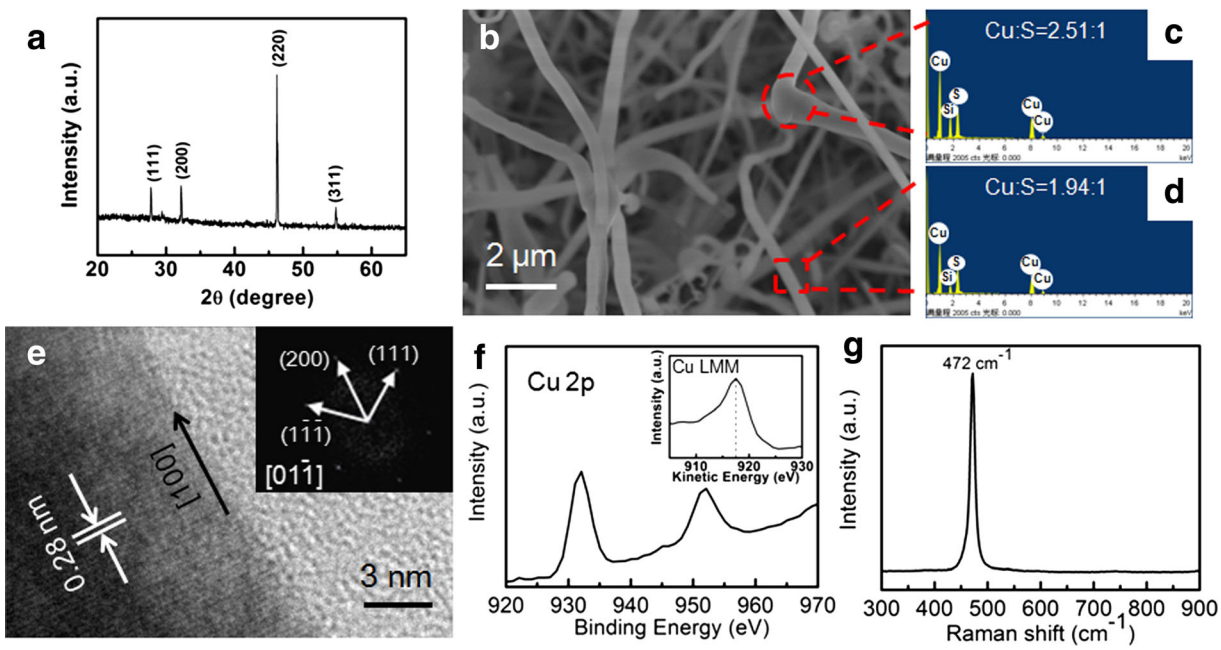

Fig. 2 Typical characterizations of the products synthesized at 700 °C with the chamber pressure 700 Torr, using a mixture gas of Ar (10 sccm) and H_2 (50 sccm) as the carrier gas. **a** XRD pattern. **b** SEM image. **c**, **d** EDS spectra from the corresponding zone marked in **b**. **e** HRTEM image, *inset* shows the corresponding FFT pattern. **f** Cu 2p XPS spectrum and the Cu LMM Auger spectrum (*inset*). **g** Raman spectrum

up to 50 μm (mostly 5–20 μm) and diameter in the range of 100–500 nm, some of which have remarkable particles at their ends. EDS spectra taken from the end and the middle of nanowires are shown in Fig. 2c, d, respectively. The atomic ratio of Cu:S from the middle of the nanowires is revealed to be about 1.94:1, which is similar to the stoichiometry of Cu_2S, while the end of the nanowires is remarkably rich in Cu (atomic ratio of Cu:S to be about 2.51:1), which may imply a metal-catalyzed growth of the Cu_2S nanowires. HRTEM image and the corresponding fast Fourier transformation (FFT) pattern taken from the edge of a single Cu_2S nanowire (Fig. 2e) disclose a well-defined 2D lattice fringe with the interplanar spacing 0.28 nm, which is consistent with the lattice plane (200) of face-centered Cu_2S. Therefore, we can deduce that as-synthesized nanowires grow along the direction (100).

Figure 2f shows the Cu 2p core level XPS spectrum and the Cu LMM Auger spectrum. The modified Auger parameter (α'), defined as the sum of the kinetic energy of the Auger signal and the binding energy of the photoelectron line, can be calculated to be 1849.6 eV, suggesting the monovalence state of copper, i.e., Cu(I) (Yu et al. 2013). Meanwhile, the Raman spectrum (Fig. 2g) shows a characteristic Raman peak at 472 cm^{-1}, which is also consistent with the results reported for Cu_2S nanostructures (Lai et al. 2010a, b). Since Cu_2S will be the product whenever a cuprous salt is reacted with H_2S or Na_2S (Roberts and Buchanan 1971), H_2 is added to the carrier gas so as to convert S into H_2S. Cu_2S will be synthesized according to the following equation (Bierman et al. 2007):

$$H_2 + S \rightarrow H_2S$$

$$2CuCl + H_2S \rightarrow Cu_2S + 2HCl$$

Cu_2S formed in the vapor phase will be transferred by the carrier gas to downstream position of the tube furnace with gradually decreased temperature and deposited there.

However, due to the small Gibbs free energy $\triangle G^{\theta}$ of the reaction ($Cu_2S + S \rightarrow 2CuS$), Cu_2S will spontaneously transform into CuS when there is excess S. Therefore, the content of H_2 will be crucial to the synthesis of single phase Cu_2S. For comparing, the reaction has been carried out with different carrier gas. When pure Ar was used as the carrier gas, no products were formed on the Si substrate. When the mixture gas of Ar and H_2 (5%) was used, the products are mostly quasi hexagonal nanoflakes (see in Fig. 3), which reminds us the typical morphology of covellite CuS, easily existing in hexagonal flakes due to the intrinsic structural features of stacked CuS_4–CuS_3–CuS_4 layers that are held together by covalent S–S bonds (Wu et al. 2006a, b). XRD pattern and EDS spectrum further reveal them to be hexagonal CuS (JCPDS card no. 6-464), which is well expected.

The chamber pressure during deposition is proved to be the other important factor for the successful synthesis of Cu_2S nanowires. Figure 4 shows the typical SEM images of the products obtained at different chamber pressure. Typical octahedron and truncated octahedron with size 25–50 μm were formed at a low pressure (Fig. 4a, b). With the increase of the pressure, the size of products decreased remarkably, and quasi 1D nanostructures will be the main products when the pressure is over 500 Torr (Fig. 4e, f). We suggest that the pressure-dependent crystal growth can be ascribed to the differential of the precursor concentration (Li et al. 2011). Due to the high vapor pressure of CuCl and S, Cu_2S was easily formed in the vapor phase. When the reaction was carried out at a lower chamber pressure, the supersaturation of Cu_2S in the vapor phase was relatively higher which will surpass the surface energy barrier and favor the isotropic growth, giving rise to 0D polyhedrons. While at higher pressure, the anisotropic growth will be gradually dominant.

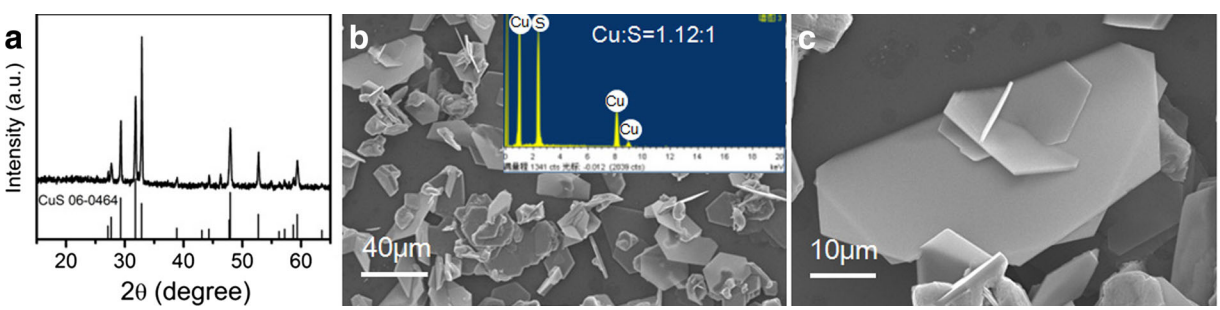

Fig. 3 **a** XRD pattern and **b**–**c** SEM images of the products synthesized using the mixture gas of Ar and H_2 (5%) as the carrier gas (temperature 700 °C, chamber pressure 700 Torr). *Inset* in **b** shows the corresponding EDS spectrum

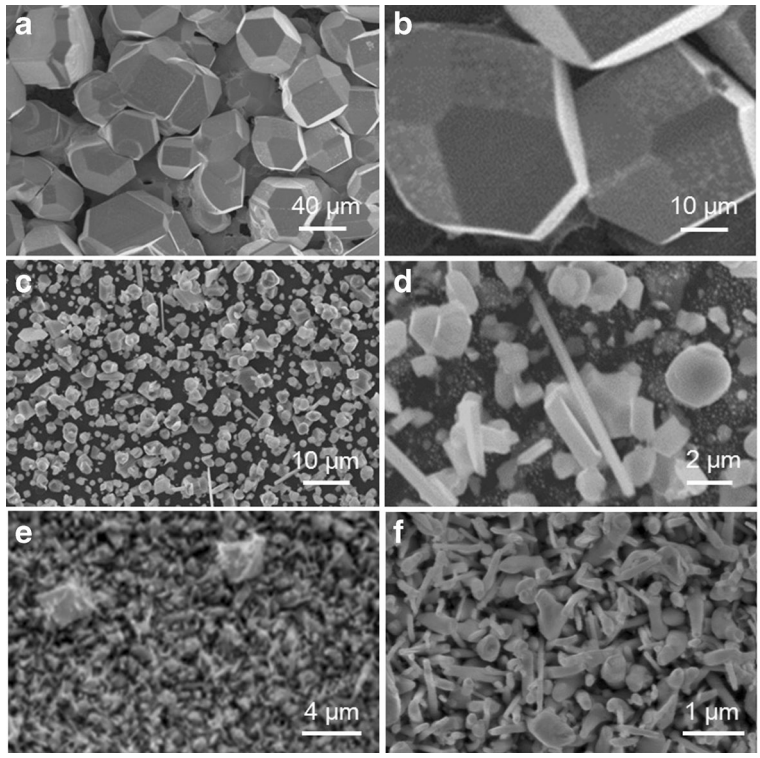

Fig. 4 SEM images of the products synthesized under different chamber pressure (700 °C, carrier gas: the mixture gas of 10 sccm Ar and 50 sccm H_2). **a**, **b** 100 Torr. **c**, **d** 300 Torr. **e**, **f** 500 Torr

Vapor-liquid-solid (VLS) mechanism is well known to account for the growth of quasi 1D semiconductor nanostructures via CVD method which uses metal particles such as Au as the catalyst (Luo et al. 2014a, b). No catalyst particles were precoated to the Si substrate during our experiments. Therefore, we deduce that trace element Cu reduced by H_2 may serve as the catalyst (Xu et al. 2012), which has also been proved by the Cu-rich particles existing at the end of the Cu_2S nanowires.

FETs based on a single Cu_2S nanowire were then fabricated for the electrical characterization. As illustrated in Fig. 5a, metal Au was selected as the electrode material. The linear current versus voltage (*I*–*V*) curve of a Cu_2S nanowire (Fig. 5b) in dark reveals a good Ohmic contact, and the conductivity of the Cu_2S nanowires is deduced to be about 600 S cm^{-1}, which is comparable with that of CuS nanotubes (Wu et al. 2013). Figure 5c shows the transport properties of the Cu_2S nanowires. The source-drain current (I_{ds}) versus source-drain voltage (V_{ds}) curves were measured under varied gate voltage V_g from −40 to +40 V with a step of 40 V. The decrease of conductance with the increasing V_g confirms the p-type characteristic of the Cu_2S nanowires. However, the weak gate effect may be attributed to the high conductivity of the Cu_2S nanowires (Wu et al. 2013).

The field-effect hole mobility (μ_h) and the hole concentration (n_h) of the Cu_2S nanowires can be further estimated according to the following equations:

$$\mu_h = g_m \frac{\ln(4h/d)L}{2\pi\varepsilon_0\varepsilon_{SiO_2}V_{ds}},$$

where transconductance ($g_m = dI_{ds}/dV_g$) is extracted from the linear region of the I_{ds}–V_g curve. L is the channel length, d is the nanowire diameter, ε_{SiO_2} is the dielectric constant of the SiO_2 dielectric (~3.9), and h is the thickness of the SiO_2 dielectric. The hole mobility (μ_h) is calculated to be about 72 cm^2 V^{-1} s^{-1}, which is well consistent with the reported value of Cu_2S thick film (Sorokin and Paradenko 1966). Furthermore, the hole concentration (n_h) is deduced to be about 5×10^{19} cm^{-3} through the equation $n_h = \sigma/q\mu_h$, where σ is the conductivity of the nanowires and q is the elementary charge. Figure 5d shows the UV–vis–NIR absorption spectrum of the as-synthesized Cu_2S nanowires on Si substrate, which presents a near-band-edge (NBE) absorption peak at 424 nm and a stronger near-

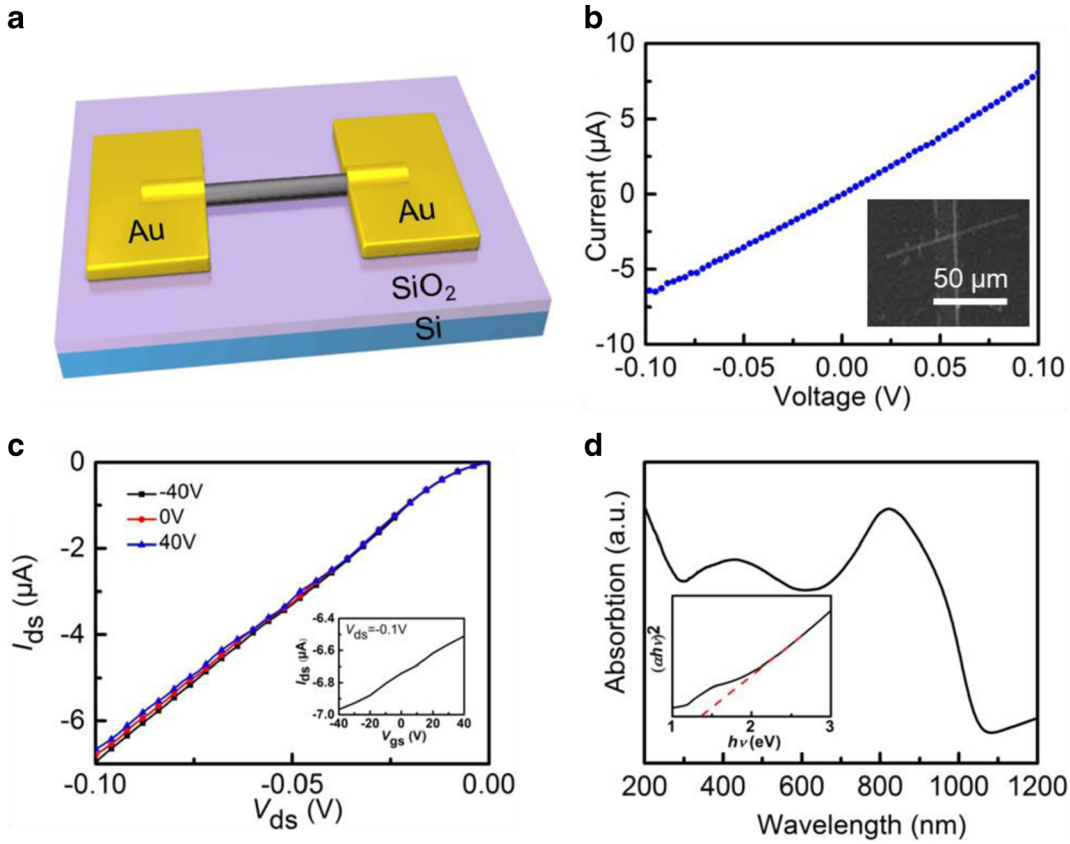

Fig. 5 **a** Schematic illustration of the bottom-gate FET based on a single Cu_2S nanowire. **b** The typical *I–V* curve of a single Cu_2S nanowire in dark. *Inset* shows the SEM image of a typical nanodevice. **c** I_{ds}–V_{ds} curves measured with V_g increasing from −40 to 40 V with a step of 40 V. The *inset* shows the corresponding I_{ds}–V_g curve at V_{ds} = −0.1 V. **d** UV–vis–NIR absorption spectrum of the as-synthesized Cu_2S nanowires on Si substrate. *Inset* shows the corresponding $(\alpha h\nu)^2$–$h\nu$ plot

infrared (NIR) absorption peak at 815 nm. From the corresponding $(\alpha h\nu)^2$–$h\nu$ plot (inset of Fig. 5d), the optical band gap of the as-synthesized Cu_2S nanowires is deduced to be about 1.37 eV. The strong absorption in NIR range corresponds to the localized surface plasmon resonances (LSPR) due to the relatively high carrier (holes) concentration in the as-synthesized products, which is well reported for the copper chalcogenides (Luther et al. 2011). Meanwhile, the strong absorption in NIR range reminds us the application of Cu_2S/Si heterojunction in the field of NIR photodetector.

To fabricate an NIR photodetector, the above Cu_2S nanowire network was then deposited on the n-type Si substrate to form a relatively dense layer, which can form the p-Cu_2S nanowires/n-Si heterojunction. Afterwards, Au (50 nm) electrode was deposited onto the as-grown Cu_2S layer as a top Ohmic contact electrode with a shadow mask. A bottom Ohmic contact was formed by coating eutectic In:Ga onto the reverse of the n-Si substrate. Figure 6b shows the typical *I–V* curve of the heterojunction (S = 0.25 cm^2) measured in dark, displaying distinct rectifying characteristics with a turn-on voltage of ~0.6 V and a rectification ratio of ~300. When the heterojunction was illuminated by the NIR light (790 nm, 0.35 mW cm^{-1}), a pronounced photovoltaic behavior with the open circuit voltage (V_{oc}) 0.09 V and the short circuit current (I_{sc}) 65 nA can be observed (Fig. 6c), revealing the potential of the as-synthesized Cu_2S nanowires in the field of self-driven NIR photodetector (Luo et al. 2014a, b). As shown in Fig. 6d, the heterojunction shows high sensitivity to the incident light with an I_{on}/I_{off} ratio >600 and a fast response speed <0.5 s (limited by the speed of manually turning on and off the light) at zero external bias, implying that the electron-hole pairs could be effectively generated and separated in the Cu_2S/Si heterojunction. Moreover, the device exhibits excellent reproducibility and stability under pulsed light

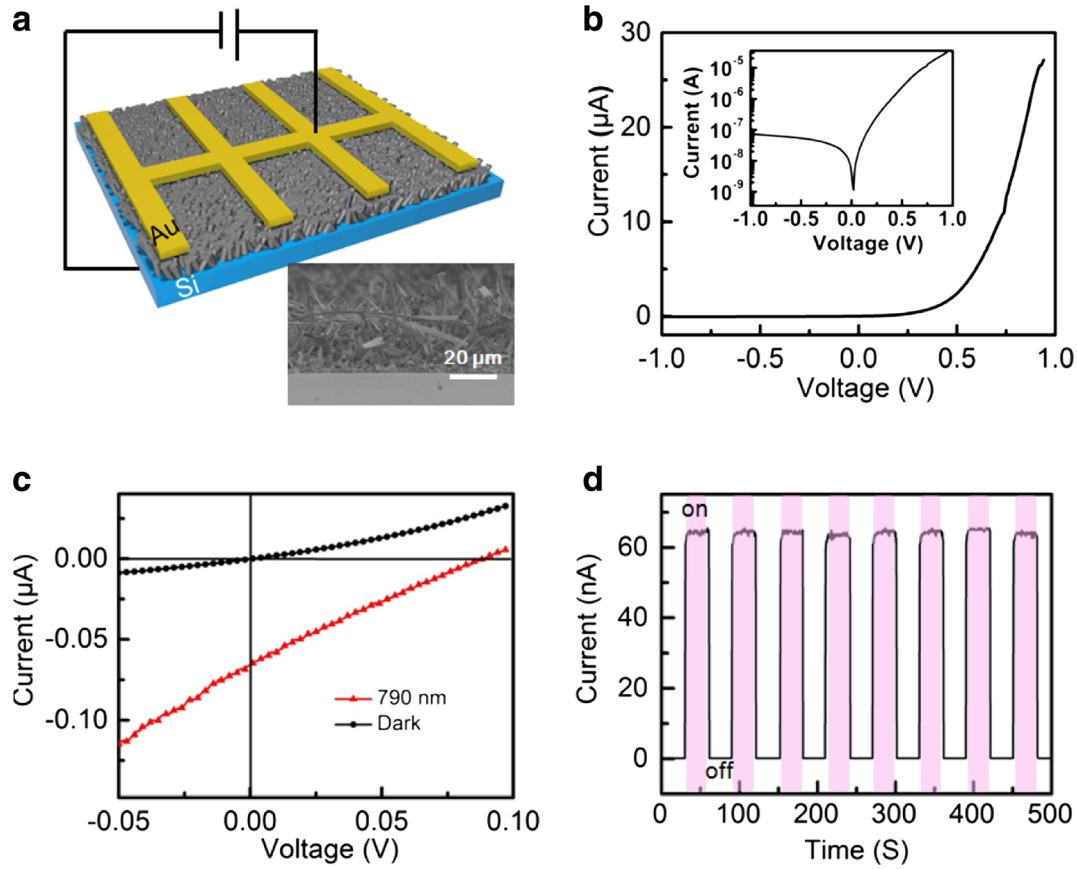

Fig. 6 Electrical characterization of the p-Cu_2S nanowires/n-Si heterojunction. **a** Schematic illustration. **b** Typical *I–V* curve in dark. *Inset* shows the corresponding semilogarithmic plot. **c** *I–V* curves in the dark and under NIR light illumination (790 nm, 0.35 mW cm^{-2}). **d** Time response to pulsed light at zero bias

illumination, indicating that the device can function as a high-performance photovoltaic-type photodetector.

Responsivity (R) and specific detectivity (D^*) are normally used to delineate the photodetectors performance, which can be described according to the following equations (Wu et al. 2012)

$$R\left(\mathrm{A\ W^{-1}}\right) = \frac{I_p - I_d}{SP_{opt}}$$

$$D^*\left(\mathrm{cm\ Hz^{1/2}\ W^{-1}}\right) = \frac{S^{\frac{1}{2}}R}{(2qI_d)^{\frac{1}{2}}},$$

where I_p is the photocurrent, I_d is the dark current, P_{opt} is the incident light power, S is the area of the effective junction area, and q is the charge of an electron. Based on the above values, R and D^* are estimated to be about 0.8 mA W^{-1} and 6.7×10^{10} cm $Hz^{1/2}$ W^{-1}, respectively. As we can see from Table 1, the as-fabricated Cu_2S/Si heterojunction has a comparable specific D^* to other Si-based heterojunctions self-driven photodetectors.

Table 1 Summary of key metrics of Si-based heterojunctions NIR photodetectors

Photodetector	R (mA W^{-1})	I_p/I_d	D^* (cm $Hz^{1/2}$ W^{-1})	Ref
p-Cu_2S/n-Si wafer	0.8	600	6.7×10^{10}	This work
p-CuO/n-Si arrays	64	560	7.6×10^{8}	Hong et al. 2014
n-CdS/p-Si arrays	110	21	1.86×10^{11}	Manna et al. 2012
MLG/n-Si wafer	29	10^4	3.9×10^{11}	Lv et al. 2013

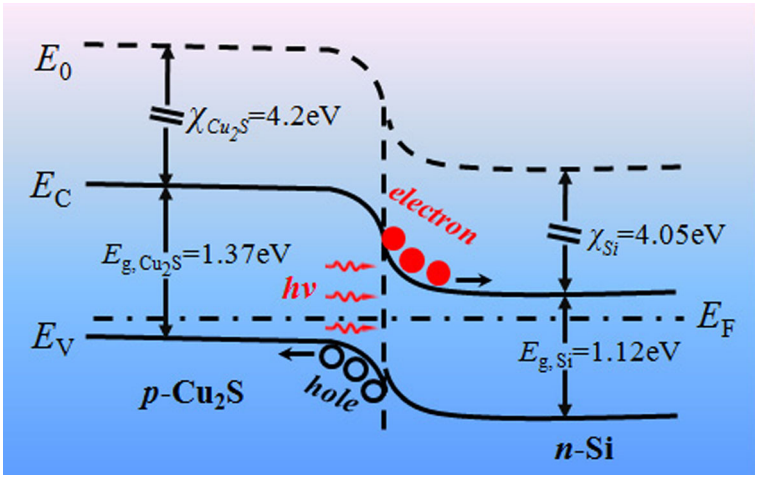

Fig. 7 Energy band diagram of the p-Cu_2S/n-Si heterojunction upon light illumination

However, the lower *R* may be attributed to the limited absorption of Si wafer compared to Si nanowire arrays used in the other devices.

The mechanism of the NIR photodetector can be well elucidated by the energy band diagram of the p-Cu_2S nanowires/n-Si heterojunction presented in Fig. 7. A space-charge region is formed between p-Cu_2S and n-Si, with the built-in electric field directing from Si to Cu_2S. When the heterojunction is illuminated by an incident NIR light, a massive amount of electron-hole pairs will be excited due to the efficient absorption by both Cu_2S and Si. The photogenerated electron-hole pairs are then separated by the built-in electric field in opposite directions, leading to a photocurrent in the circuit.

Conclusion

In summary, face-centered cubic Cu_2S nanowires with length up to 50 μm (mostly 5–20 μm) and diameters in the range of 100–500 nm were successfully synthesized through a chemical vapor deposition method. H_2 in the carrier gas and the higher chamber pressure are proved to be crucial to the controllable synthesis of Cu_2S nanowires, and the growth mechanism is deduced to be the VLS mechanism, using element Cu reduced by H_2 as the catalyst. The as-synthesized Cu_2S nanowires are characterized to be p-type semiconductor with the conductivity about 600 S cm^{-1} and the hole mobility (μ_h) about 72 cm^2 V^{-1} s^{-1}. Meanwhile, the p-Cu_2S nanowires/n-Si heterojunction shows a pronounced photovoltaic behavior when illuminated by the NIR light (790 nm), revealing the as-synthesized Cu_2S nanowires using to be potential materials for self-driven NIR photodetector.

Acknowledgements This work was supported by the Natural Science Foundation of China (NSFC, nos. 21501038, 61575059), the Natural Science Foundation of Anhui Province of China (nos. 1408085MB31, J2014AKZR0036), and the Fundamental Research Funds for the Central Universities (nos. 2012HGCX0003, 2013HGXJ0195, 2013HGCH0012, 2014HGCH0005).

Compliance with ethical standards

Conflict of interest The authors have declared that no conflict of interest exists.

References

Adelifard M, Eshghi H, Mohagheghi MMB (2012) An investigation on substrate temperature and copper to sulphur molar ratios on optical and electrical properties of nanostructural CuS thin films prepared by spray pyrolysis method. Appl Surf Sci 258:5733–5738

An L, Zhou PP, Yin J, Liu H, Chen FJ, Liu HY, Du YP, Xi PX (2015) Phase transformation fabrication of a Cu_2S nanoplate as an efficient catalyst for water oxidation with glycine. Inorg Chem 54:281–3289

Bierman MJ, Lau Y, Jin S (2007) Hyperbranched PbS and PbSe nanowires and the effect of hydrogen gas on their synthesis. Nano Lett 7:2907–2912

Bierman MJ, Lau AYK, Kvit AV, Schmitt AL, Jin S (2008) Dislocation-driven nanowire growth and Eshelby twist. Science 320:1060–1063

Bo XJ, Bai J, Wang LX, Guo LP (2010) In situ growth of copper sulfide nanoparticles on ordered mesoporous carbon and their application as nonenzymatic amperometric sensor of hydrogen peroxide. Talanta 81:339–345

Fahrenbruch AL, Bube RH (1983) Fundamentals of solar cells. Academic Press, New York

Feng XP, Li YX, Liu HB, Li YL, Cui S, Wang N, Jiang L, Liu XF, Yuan MJ (2007) Controlled growth and field emission properties of CuS nanowalls. Nanotechnology 18:145706

Garnett EC, Tseng YC, Khanal DR, Wu JQ, Bokor J, Yang PD (2009) Dopant profiling and surface analysis of silicon nanowires using capacitance-voltage measurements. Nat Nanotechnol 4:311–314

Ghahremaninezhad A, Asselin E, Dixon DG (2011) Electrodeposition and growth mechanism of copper sulfide nanowires. J Phys Chem C 115:9320–9334

Hong QS, Cao Y, Xu J, Lu HM, He JH, Sun JL (2014) Self-powered ultrafast broadband photodetector based on p-n heterojunctions of CuO/Si nanowire array. ACS Appl Mater Interfaces 6:20887–20894

Lai CH, Huang KW, Cheng JH, Lee CY, Hwang BJ, Chen LJ (2010a) Direct growth of high-rate capability and high capacity copper sulfide nanowire array cathodes for lithium-ion batteries. J Mater Chem 20:6638–6645

Lai CX, Wu QB, Chen J, Wen LS, Ren S (2010b) Large-area aligned branched Cu_2S nanostructure arrays: room-temperature synthesis and growth mechanism. Nanotechnology 21:15602

Li WH, Shavel A, Guzman R, Rubio-Garcia J, Flox C, Fan JD, Cadavid D, Ibanez M, Arbiol J, Morante JR, Cabot A (2011) Morphology evolution of $Cu_{2-x}S$ nanoparticles: from spheres to dodecahedrons. Chem Commun 47:10332–10334

Lim WP, Wong CT, Ang SL, Low HY, Chin WS (2006) Phase-selective synthesis of copper sulfide nanocrystals. Chem Mater 18:6170–6177

Liu ZP, Xu D, Liang LB, Shen JM, Zhang SY, Qian YT (2005) Growth of Cu_2S ultrathin nanowires in a binary surfactant solvent. J Phys Chem B 109:10699–10704

Luo LB, Chen JJ, Wang MZ, Hu H, Wu CY, Li Q, Wang L, Huang JA, Liang FX (2014a) Near infrared light photovoltaic detector based on GaAs nanocones array/monolayer graphene Schottky junction. Adv Funct Mater 24:2794–2800

Luo LB, Huang XL, Wang MZ, Xie C, Wu CY, Hu JG, Wang L, Huang JA (2014b) The effect of plasmonic nanoparticles on the optoelectronic characteristics of CdTe nanowires. Small 10:2645–2652

Luther JM, Jain PK, Ewers T, Alivisatos AP (2011) Localized surface plasmon resonances arising from free carriers in doped quantum dots. Nat Mater 10:361–366

Lv P, Zhang XJ, Zhang XW, Deng W, Jie JS (2013) High-sensitivity and fast-response graphene/crystalline silicon Schottky junction-based near-IR photodetectors. IEEE Electron Dev Lett 34:1337–1339

Manna S, Das S, Mondal SP, Singha R, Ray SK (2012) High efficiency Si/CdS radial nanowire heterojunction photodetectors using etched Si nanowire templates. J Phys Chem C 116:7126–7133

Mu CF, Yao QZ, Qu XF, Zhou GT, Li ML, Fu SQ (2010) Controlled synthesis of various hierarchical nanostructures of copper sulfide by a facile microwave irradiation method. Colloids Surf A Physicochem Eng Asp 371:14–21

Roberts WMB, Buchanan AS (1971) The effect of temperature, pressure, and oxygen on copper and iron sulphides synthesized in aqueous solution. Mineral Deposita 6:23–33

Sorokin GP, Paradenko AP (1966) Electrical properties of Cu_2S. Sov Phys J 9:59–61

Su YJ, Lu XN, Xie MM, Geng HJ, Wei H, Yang Z, Zhang YF (2013) A one-pot synthesis of reduced graphene oxide-Cu_2S quantum dot hybrids for optoelectronic devices. Nanoscale 5: 8889–8893

Thongtem T, Phuruangrat A, Thongtem S (2010) Characterization of copper sulfide nanostructured spheres and nanotubes synthesized by microwave-assisted solvothermal method. Mater Lett 64:136–139

Tian QW, Tang MH, Sun YG, Zou RJ, Chen ZG, Zhu MF, Yang SP, Wang JL, Wang JH, Hu JQ (2011) Hydrophilic flower-like CuS superstructures as an efficient 980 nm laser-driven photothermal agent for ablation of cancer cells. Adv Mater 23:3542–3547

Wang SH, Yang SH (2001) Growth of crystalline Cu_2S nanowire arrays on copper surface: effect of copper surface structure, reagent gas composition, and reaction temperature. Chem Mater 13:4794–4799

Wang SY, Huang CW, Lee DY, Tseng TY, Lin CY (2009) Multilevel resistive switching in Ti/Cu_xO/Pt memory devices. J Appl Phys 108:114110

Wang KJ, Li GD, Li JX, Wang Q, Chen JS (2007) Formation of single-crystalline CuS nanoplates vertically standing on flat substrate. Cryst Growth Des 7:2265–2267

Wu D, Jiang Y, Zhang YG, Yu YQ, Zhu ZF, Lan XZ, Li FZ, Wu CY, Wang L, Luo LB (2012) Self-powered and fast-speed photodetector based on CdS:Ga nanoribbon/Au Schottky diodes. J Mater Chem 22:23272–23276

Wu ZC, Pan C, Yao ZY, Zhao QR, Xie Y (2006a) Large-scale synthesis of single-crystal double-fold snowflake Cu_2S dendrites. Cryst Growth Des 6:1717–1719

Wu C, Shi JB, Chen CJ, Chen YC, Lin YT, Wu PF, Wei SY (2008) Synthesis and optical properties of CuS nanowires fabricated by electrodeposition with anodic alumina membrane. Mater Lett 62:1074–1077

Wu CY, Yu SH, Antonietti M (2006b) Complex concaved cuboctahedrons of copper sulfide crystals with highly geometrical symmetry created by a solution process. Chem Mater 18:3599–3601

Wu CY, Zhang ZH, Wu YL, Lv P, Nie B, Luo LB, Wang L, Hu JG, Jie JS (2013) Flexible CuS nanotubes–ITO film Schottky junction solar cells with enhanced light harvesting by using an Ag mirror. Nanotechnology 24:045402

Xiong HM, Cheng MH, Zhou Z, Zhang X, Shen JC (1998) A new approach to the fabrication of a self-organizing film of heterostructured polymer/Cu_2S nanoparticles. Adv Mater 10:529–532

Xu M, Wu HY, Da PM, Zhao DY, Zheng GF (2012) Unconventional 0-, 1-, and 2-dimensional single-crystalline copper sulfide nanostructures. Nanoscale 4:1794–1799

Yu YQ, Jiang Y, Jiang P, Zhang YG, Wu D, Zhu ZF, Liang Q, Chen SR, Zhang Y, Jie JS (2013) Large conductance switching nonvolatile memories based on p-ZnS nanoribbon/n-Si heterojunction. J Mater Chem C 1:1238–1244

Zhai TY, Li L, Ma Y, Liao MY, Wang X, Fang XS, Yao JN, Bando YS, Golberg D (2011) One-dimensional inorganic nanostructures: synthesis, field-emission and photodetection. Chem Soc Rev 40:2986–3004

Zhang WX, Wen XG, Yang SH (2003) Synthesis and characterization of uniform arrays of copper sulfide nanorods coated with nanolayers of polypyrrole. Langmuir 19:4420–4426

Zhao YX, Pan HC, Lou YB, Qiu XF, Zhu JJ, Burda C (2009) Plasmonic Cu2-xS nanocrystals: optical and structural properties of copper-deficient copper(I) sulfides. J Am Chem Soc 131:4253–4261